22nd IBERIAN LATIN-AMERICAN CONGRESS ON COMPUTATIONAL METHODS IN ENGINEERING
2nd Brazilian Congress on Computational Mechanics
NOVEMBER 7-9, 2001
Campinas, SP - Brazil

ON THE STRONG DISCONTINUITY APPROACH IN 3D SETTINGS

Chaves, E. W. V.
E.T.S. Enginyers de Camins, Canals i Ports. – Technical University of Catalonia (UPC) - Campus Nord UPC Módulo C-1 – Gran Capitán s/n, 08034 – Barcelona – Spain
e-mail: chaves@cimne.upc.es
Web: www.rmee.upc.es/homes/chaves

Oliver, J.
E.T.S. Enginyers de Camins, Canals i Ports. – Technical University of Catalonia (UPC) - Campus Nord UPC Módulo C-1 – Gran Capitán s/n, 08034 – Barcelona – Spain
e-mail: oliver@cimne.upc.es

Abstract. The paper deals with the extension of the two-dimensional Strong Discontinuity Approach (SDA) to the general 3D case on the basis of isotropic continuum damage models. A variable bandwidth model defines the transition from weak to strong discontinuity regimes. The bifurcation analysis provides the ingredients to determine the propagation of the discontinuity across the body. The basic ingredients of a 3D finite element with an embedded discontinuity are also presented. In order to illustrate the effectiveness of the method several numerical simulations are performed.

Keywords: Strong Discontinuity, Damage, Localization, Bifurcation.

1 INTRODUCTION

During the last decades, research on the simulation of the post-peak behavior of materials has made important progress. In many cases, the observed post-peak softening behavior is associated to the onset and progression of macroscopical discontinuities (jumps in the displacement fields) which, depending on the context, are called cracks, slip-lines etc. Several theories have provided theoretical basis for the simulation of the onset and propagation of cracks in materials both at macroscopic and microscopic levels. In general, the available models can be classified into two families: *Fracture Mechanics models*, Rice (1976), Ingrafea & Saouma (1985) and *Continuum Mechanics models*. In the context of Continuum Mechanics based models a new method has recently emerged: the *Strong Discontinuity Approach* (SDA). This method is based on the use of standard stress-strain continuum constitutive equations to induce a discrete (traction-displacement jump) constitutive equation at the discontinuous interface by introducing the so called *strong discontinuity kinematics* Simo & Oliver(1994a); Oliver (1996a); Armero & Garikipati (1996), Oliver *et al.* (1999). In all the cases the analysis and simulation was restricted to the two-dimensional case and generalization of the Strong Discontinuity Approach to general three-dimensional problems is the main aim of this paper.

The material's behavior associated to the development of a crack in a loading process can be described as (see Figure 1):

- ***Diffuse failure zone***: The strain and displacement fields are continuous, but there is a concentration of the strains in the zone where material begins to soften
- ***Weak discontinuity zone***: The strain field becomes discontinuous, but the displacement field remaining continuous, across the limits of a narrow band (strain localization band).
- ***Strong discontinuity zone***: The strain localization band collapses into a surface (the discontinuity interface). The displacement field becomes discontinuous across that surface and the strain field becomes unbounded.

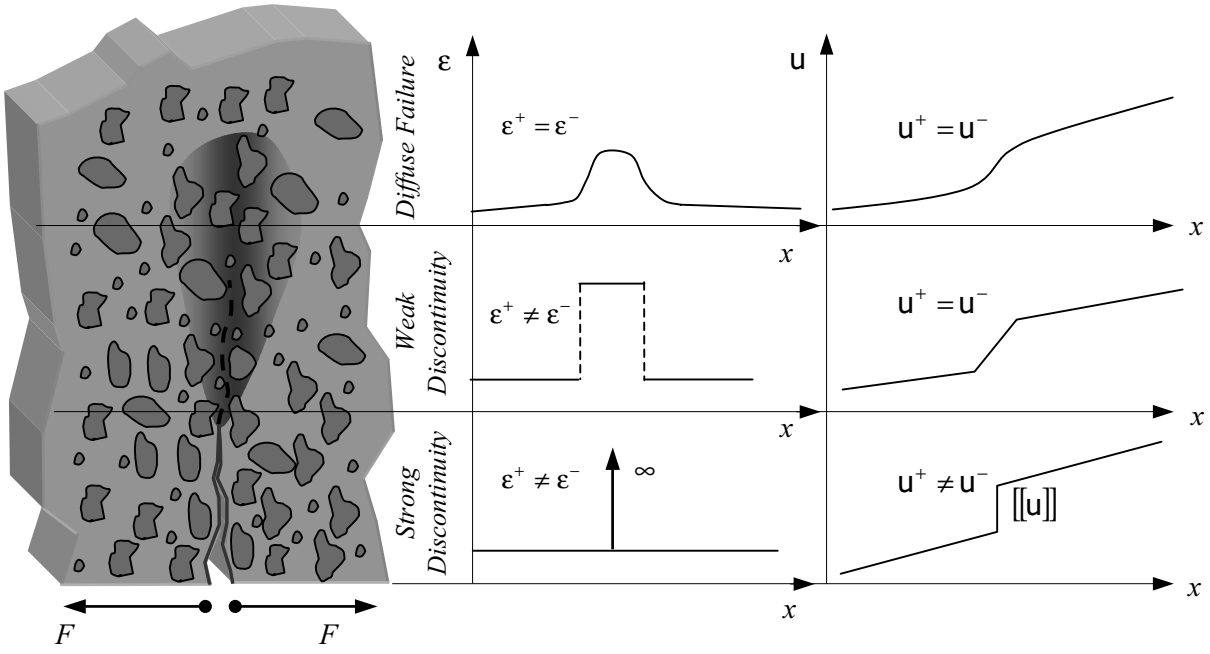

Figure 1 – Fracture process zone

2 GOVERNING EQUATIONS

Let us consider a three dimensional body, that takes up an open bounded domain $\mathcal{B} \in \mathbb{R}^3$, experiencing a displacement discontinuity across a discontinuity surface $\mathcal{S}$ of normal $\mathbf{N}$ (see Figure 2). Let $\partial\mathcal{B}$ be the boundary of $\mathcal{B}$ and $\boldsymbol{\upsilon}$ the unit normal. The body is in static equilibrium under the action of body forces, $\mathbf{b}(\mathbf{x})$, and surface tractions, $\mathbf{t}(\mathbf{x})$. The boundary $\partial\mathcal{B}$ consists of a portion $\mathcal{B}_u$ with prescribed displacements, $\mathbf{u}^*(\mathbf{x})$, and a part $\partial\mathcal{B}_t$, with prescribed tractions, $\mathbf{t}(\mathbf{x})$, such that $\partial\mathcal{B}_u \cap \partial\mathcal{B}_t = \varnothing$ and $\partial\mathcal{B}_u \cup \partial\mathcal{B}_t = \partial\mathcal{B}$. In addition let $\boldsymbol{\sigma}(\mathbf{x})$ denote the *Cauchy stress* tensor and $\boldsymbol{\varepsilon}(\mathbf{x})$ the infinitesimal strain tensor. The governing equations of a Boundary Value Problem (BVP) for the quasi-static problem under the assumption of infinitesimal deformation are summarized below:

BOUNDARY VALUE PROBLEM - BVP			
Equilibrium equation	$\nabla \cdot \boldsymbol{\sigma}(\mathbf{x}) + \mathbf{b}(\mathbf{x}) = \mathbf{0}$	$\forall\, \mathbf{x} \in \mathcal{B} / \mathcal{S}$	(1)
Constitutive equation	$\boldsymbol{\sigma} = \Xi(\boldsymbol{\varepsilon}(\mathbf{x}))$	$\forall\, \mathbf{x} \in \mathcal{B}$	(2)
Kinematic equation	$\boldsymbol{\varepsilon} = \nabla^S \mathbf{u} = \frac{1}{2}\left(\nabla \otimes \mathbf{u} + \mathbf{u} \otimes \nabla\right)$	$\forall\, \mathbf{x} \in \mathcal{B}$	(3)
Outer traction continuity	$\mathcal{T}^- = \mathcal{T}^+ \therefore\ \mathbf{N} \cdot \boldsymbol{\sigma}^- = \mathbf{N} \cdot \boldsymbol{\sigma}^+$	$\forall\, \mathbf{x} \in \mathcal{S}$	(4)
Essential boundary conditions	$\mathbf{u} = \mathbf{u}^*(\mathbf{x})$	$\forall\, \mathbf{x} \in \partial\mathcal{B}_u$	(5)
Natural boundary conditions	$\mathbf{t} = \mathbf{t}^*(\mathbf{x}) = \boldsymbol{\upsilon} \cdot \boldsymbol{\sigma}$	$\forall\, \mathbf{x} \in \partial\mathcal{B}_t$	(6)
Inner traction continuity	$\mathcal{T}^+ = \mathcal{T}_{\mathcal{S}} \therefore\ \mathbf{N} \cdot \boldsymbol{\sigma}^+ = \mathbf{N} \cdot \boldsymbol{\sigma}_{\mathbf{S}}$	$\forall\, \mathbf{x} \in \mathcal{S}$	(7)

In Eq.(2), $\Xi(\boldsymbol{\varepsilon})$ stands for the nonlinear constitutive equation returning the stresses in terms of the strains.

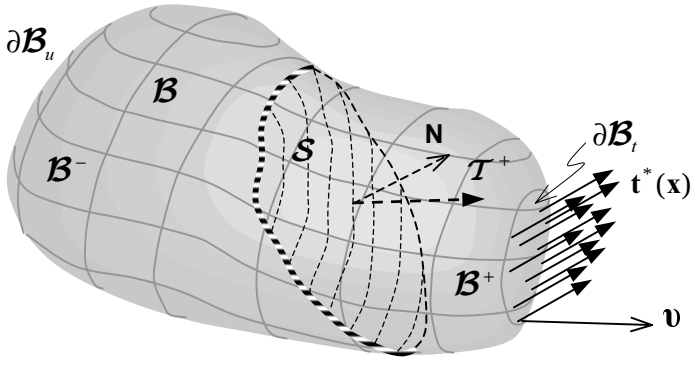

Figure 2 – Three dimensional body and discontinuous interface $\mathcal{S}$.

3 DISCONTINUOUS KINEMATICS

The kinematics of a body $\mathcal{B}$ exhibiting a discontinuity of value $[[\dot{\mathbf{u}}]](\mathbf{x},t)$ in the rate of displacement field (see Figure 2) across a material surface denoted by $\mathcal{S}$, whose normal $\mathbf{N}$ points toward $\mathcal{B}^+$, can be described as:

Displacement field
$$\dot{\mathbf{u}}(\mathbf{x},t) = \underbrace{\dot{\bar{\mathbf{u}}}(\mathbf{x},t)}_{regular} + \underbrace{H_S(\mathbf{x})[[\dot{\mathbf{u}}]](\mathbf{x},t)}_{discontinuity} \tag{8}$$

Strain field
$$\begin{cases} \dot{\boldsymbol{\varepsilon}}(\mathbf{x},t) = (\nabla \dot{\mathbf{u}})^S = \underbrace{(\nabla \dot{\bar{\mathbf{u}}})^S + H_S(\mathbf{x})(\nabla[[\dot{\mathbf{u}}]])^S}_{regular} + \underbrace{\delta_S([[\dot{\mathbf{u}}]] \otimes \mathbf{N})^S}_{\text{sin } gular} \\ \Rightarrow \dot{\boldsymbol{\varepsilon}}(\mathbf{x},t) = \dot{\bar{\boldsymbol{\varepsilon}}}(\mathbf{x},t) + \delta_S([[\dot{\mathbf{u}}]] \otimes \mathbf{N})^S \end{cases} \tag{9}$$

where $(\bullet)^S$ is the symmetric part of $(\bullet)$, H_S is the step function placed on $\mathcal{S}$ ($H_S(\mathbf{x}) = 0 \quad \forall \mathbf{x} \in \mathcal{B}^-$ and $H_S(\mathbf{x}) = 1 \quad \forall \mathbf{x} \in \mathcal{B}^+$, see Figure 2) and δ_S is the Dirac's delta function placed on $\mathcal{S}$.

A regularized version of the kinematics in equation (9) can be obtained by introducing a regularized Dirac's delta function by means of a or bandwidth parameter h and a collocation function $\chi_S(\mathbf{x})$:

$$\delta_S^h(\mathbf{x}) = \frac{1}{h}\chi_S(\mathbf{x}) \qquad \chi_S(\mathbf{x}) = \begin{cases} 1 & \forall x \in \mathcal{S} \\ 0 & \forall x \in \Omega / \mathcal{S} \end{cases} \tag{10}$$

According to values of the bandwidth h in equations (8) to (10) one can distinguish the following types of discontinuities:

- Weak discontinuities ($h \neq 0$)
- Strong discontinuities ($h = 0$)

more details can be found in Oliver (2000).

4 REPRESENTATIVE CONTINUUM DAMAGE CONSTITUTIVE MODEL

4.1 Isotropic damage model

Let us consider the following isotropic continuum damage model, Oliver *et al.* (1990):

ISOTROPIC DAMAGE MODEL		
Helmholtz free Energy	$\Psi(\boldsymbol{\varepsilon}, r) = [1 - d(r)]\Psi^0 \quad \text{with} \quad \Psi^0 = \frac{1}{2}\left(\boldsymbol{\varepsilon} : \mathbb{C}^e : \boldsymbol{\varepsilon}\right)$	(11)
Damage variable	$d(r) = 1 - \frac{q(r)}{r} \quad ; \quad q \in [r_0, 0]; \quad d \in [0,1]$	(12)
Constitutive equation	$\boldsymbol{\sigma} = \frac{\partial \Psi}{\partial \boldsymbol{\varepsilon}} = (1-d)\mathbb{C}^e : \boldsymbol{\varepsilon}$	(13)
Evolution law	$\dot{r} = \gamma \qquad \begin{cases} r \in [r_0, \infty) \\ r_0 = r\big\|_{t=0} = \frac{\sigma_u}{\sqrt{E}} \end{cases}$	(14)

Damage criterion	$F(\boldsymbol{\sigma},q) \equiv \tau_\sigma - q = \sqrt{\boldsymbol{\sigma} : \mathbb{C}^{e^{-1}} : \boldsymbol{\sigma}} - q$	(15)
Hardening rule	$\dot{q} = \mathcal{H}^d(r)\,\dot{r} \quad ; \quad \left(\mathcal{H}^d = q'(r) \le 0\right)$	(16)
Loading-unloading condition	$g < 0 \qquad \gamma \ge 0 \qquad \gamma g = 0$	(17)
Consistency condition	$\gamma \dot{g} = 0$	(18)

In equation (13) $\mathbb{C}^e = \lambda(\mathbf{1} \otimes \mathbf{1}) + 2\mu\,\mathbf{I}$ is the standard fourth-order isotropic elastic modulus tensor in function of Lamé's parameters λ, μ, $\mathbf{1} = \delta_{ij}$ is the Kronecker's Delta, and $\mathbf{I}$ is the unit tensor of fourth order, defined as $\mathbf{I} = I_{ijkl} = \frac{1}{2}\left(\delta_{ik}\delta_{jl} + \delta_{il}\delta_{jk}\right)$. The incremental constitutive equation in terms of the stress and strain rates reads:

$$\dot{\boldsymbol{\sigma}} = \mathbb{C}^d : \dot{\boldsymbol{\varepsilon}} \tag{19}$$

where the tangential material stiffness $\mathbb{C}^d$ is given by:

$$\mathbb{C}^d = \begin{cases} \mathbb{C}^e & \textit{elastic} \quad \text{(a)} \\ \xi\mathbb{C}^e - \mathcal{K}\left(\mathbb{C}^e : \mathbf{m} \otimes \mathbf{n} : \mathbb{C}^e\right) & \textit{loading} \Big/ \underbrace{\textit{unloading}}_{\dot{r}=0 \to \mathcal{K}=0} \quad \text{(b)} \end{cases} \tag{20}$$

where $\mathbf{n} = \boldsymbol{\varepsilon}$, $\mathbf{m} = \boldsymbol{\varepsilon}$ and $\begin{cases} \mathcal{K} = \dfrac{q(r) - \mathcal{H}^d r}{r^3} \\ \xi = (1-d) \end{cases}$

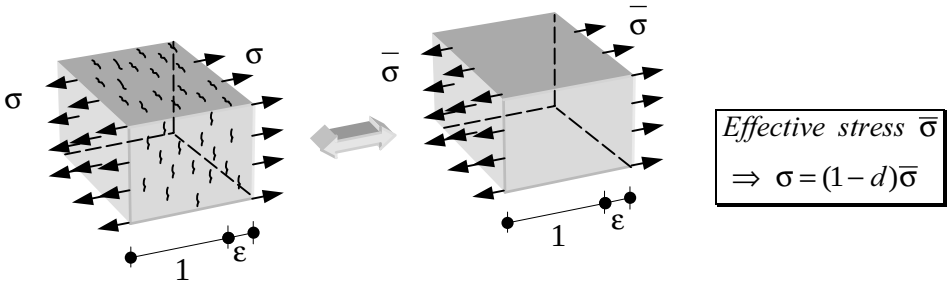

Figure 3 – Effective stress concept.

The relationship between q and r (linear or exponential softening law) are given in Figure 4.

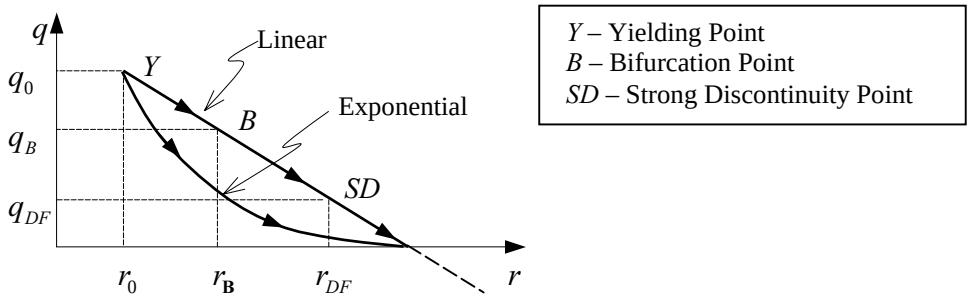

Figure 4 – Softening law.

4.2 Only-tension damage model

This model is derived from the previous isotropic damage model. The evolution of r $(\dot{r} > 0)$ is only activated upon tension in the principal stresses. This is achieved by defining the positive stress counterpart of the stress tensor:

$$\boldsymbol{\sigma}^{+} = \sum_{i=1}^{i=3} \langle \boldsymbol{\sigma}_i \rangle \mathbf{p}_i \otimes \mathbf{p}_i \tag{21}$$

where $\langle \bullet \rangle \overset{def}{=} \frac{|\bullet| + \bullet}{2}$ is the Macaulay bracket and the $\mathbf{p}_i$ stand for the elements of the principal directions base.

The tangential stiffness is given by:

$$\mathbb{C}^d = \begin{cases} \mathbb{C}^e & \text{(a)} \\ \xi \mathbb{C}^e - \boldsymbol{\kappa}\left(\overline{\boldsymbol{\sigma}}^{+} \otimes \overline{\boldsymbol{\sigma}}\right) & \text{(b)} \end{cases} \tag{22}$$

where $\boldsymbol{\sigma} = (1-d)\overline{\boldsymbol{\sigma}}$ is the relation between stress and effective stress, and the Damage Criterion is given by:

$$F^{+}\left(\boldsymbol{\sigma}^{+}, q\right) = \sqrt{\boldsymbol{\sigma}^{+} : \mathbb{C}^{e^{-1}} : \boldsymbol{\sigma}} - q \tag{23}$$

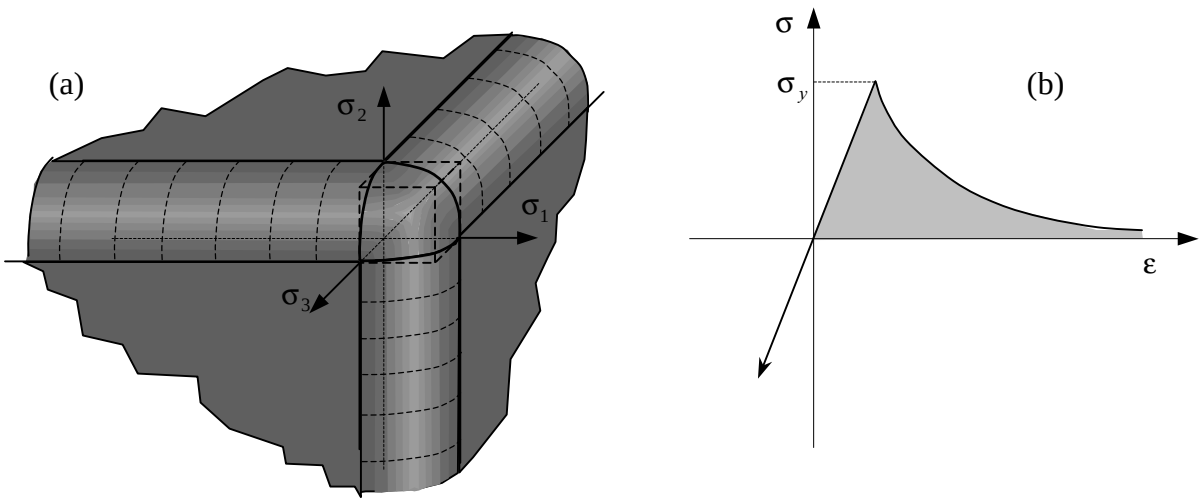

Figure 5 – Only-tension model: (a) Elastic domain in the principal stress space; (b)Stress-strain relationship in 1D.

Figure 6 schematically shows the stages of the loading process for a given material point. Point **Y** (yielding) in the figure corresponds to the initiation of the non-linear behavior. Point **B** (bifurcation) signals the onset of the discontinuous bifurcation resulting into a weak discontinuity that collapses into a strong discontinuity at Point **SD**.

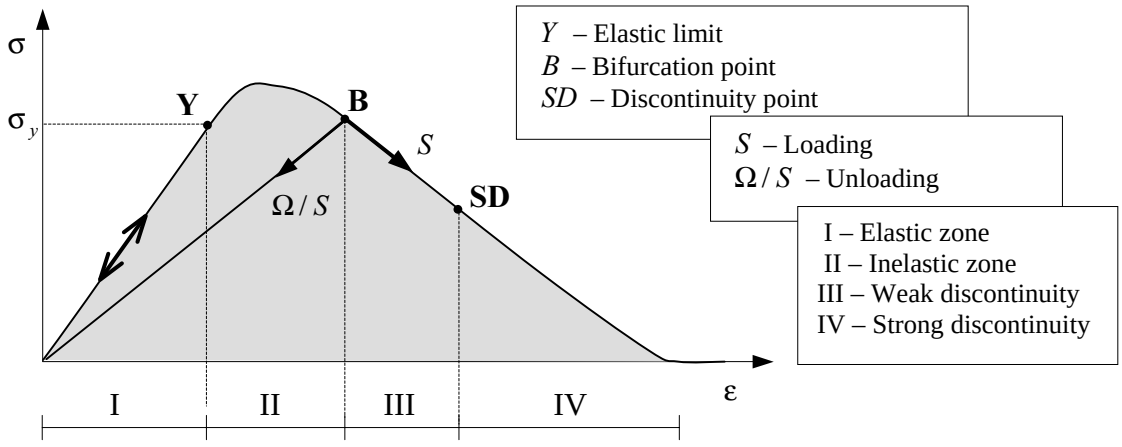

Figure 6 – Characteristic points during the loading process.

5 BIFURCATION ANALYSIS

The bifurcation of the stress-strain is signaled by the singularity of the so-called acoustic tensor $\mathbf{Q}(\mathbf{N}) = \mathbf{N} \cdot \mathbb{C}^d \cdot \mathbf{N}$ and, thus, determined by the condition $\det\mathbf{Q}(\mathbf{N}_{crit}) = 0$, see Rudnicki&Rice(1975), Willam(2000), Bigoni(2000). This Section is devoted to obtaining the bifurcation directions $(\mathbf{N}_{crit})$ and the critic hardening parameter, $\mathcal{H}^d_{crit}(\mathbf{N}_{crit})$, for the *Only-tension* damage model sketched above.

The *localization tensor* $\mathbf{Q}(\mathbf{N})$,is given from Eq. (22) by:

$$\begin{aligned} \mathbf{Q}(\mathbf{N}) = \mathbf{N} \cdot \mathbb{C}^d \cdot \mathbf{N} &= \xi \left[\mathbf{N} \cdot \mathbb{C}^e \cdot \mathbf{N} - \frac{\mathcal{K}}{\xi} \mathbf{N} \cdot \left(\mathbb{C}^e : \mathbf{m} \otimes \mathbf{n} : \mathbb{C}^e \right) \cdot \mathbf{N} \right] \\ \mathbf{Q}(\mathbf{N}) &= \xi \left[\mathbf{Q}^0 - \frac{\mathcal{K}}{\xi} \mathbf{a} \otimes \mathbf{b} \right] \end{aligned} \tag{24}$$

where $\mathbf{m} = \mathbb{C}^{e^{-1}} : \bar{\boldsymbol{\sigma}}$ and $\mathbf{n} = \mathbb{C}^{e^{-1}} : \bar{\boldsymbol{\sigma}}^+$ are coaxial tensors (they share the same principal directions) and:

$$\mathbf{Q}^0(\mathbf{N}) = \mathbf{N} \cdot \mathbb{C}^e \cdot \mathbf{N} = \mu \mathbf{1} + (\lambda + \mu) \mathbf{N} \otimes \mathbf{N} \quad \Rightarrow \quad \mathbf{Q}^{0^{-1}}(\mathbf{N}) = \frac{1}{\mu} \left[\mathbf{1} - \frac{(\lambda + \mu)}{(\lambda + 2\mu)} \mathbf{N} \otimes \mathbf{N} \right]$$

$$\mathbf{a} = \left[\lambda \mathbf{N} \operatorname{tr}(\mathbf{m}) + 2\mu \mathbf{N} \mathbf{m} \right]$$

$$\mathbf{b} = \left[\lambda \mathbf{N} \operatorname{tr}(\mathbf{n}) + 2\mu \mathbf{N} \mathbf{n} \right]$$

After some mathematical manipulations, we can obtain the bifurcation condition as:

$$\det\mathbf{Q}(\mathbf{N}) = \det \xi \mathbf{Q}^0 \left[\mathbf{1} - \frac{\mathcal{K}}{\xi} \underbrace{(\mathbf{a} \cdot \mathbf{Q}^{0^{-1}})}_{\mathbf{c}} \otimes \mathbf{b} \right] = 0 \tag{25}$$

Eq. (25) yields:

$$\det[\mathbf{Q}(\mathbf{N})] = \xi \det\left(\mathbf{Q}^0\right) \det\left[\mathbf{1} - \frac{\mathcal{K}}{\xi} \mathbf{c} \otimes \mathbf{b} \right] = 0 \tag{26}$$

Since $\mathbf{Q}^0(\mathbf{N})$ can be proved to be positive definite, and using the identity $\det[\mathbf{1} + \mathbf{c} \otimes \mathbf{b}] = 1 + \mathbf{c} \cdot \mathbf{b}$, the problem reads:

$$\det\left[\mathbf{1}-\frac{\mathcal{K}}{\xi}\mathbf{c}\otimes\mathbf{b}\right]=1-\frac{\mathcal{K}}{\xi}\mathbf{a}\cdot\mathbf{Q}^{0^{-1}}\cdot\mathbf{b}=0 \tag{27}$$

From Eq. (27) the values of the softening $\mathcal{H}^d(\mathbf{N})$, that make singular the localization tensor, can be extracted and they are given in Eq. (28)a. Then, the values $\mathbf{N}=\mathbf{N}_{crit}$, that maximize $\mathcal{H}^d(\mathbf{N})$, can be extracted through a maximization analysis. Finally, the critical (maximum) value of the softening parameter $\mathcal{H}^d_{crit}=\mathcal{H}^d(\mathbf{N}_{\mathbf{crit}})$ can be computed as it is given in Eq. (28)b:

$$\mathcal{H}^d(\mathbf{N})=\xi\left(1-\frac{r^2}{\mathbf{a}\cdot\mathbf{Q}^{0^{-1}}\cdot\mathbf{b}}\right) \quad \text{(a)}$$

$$\mathbf{N}=\mathbf{N}^{crit}$$

$$\mathcal{H}^d_{crit}=\xi\left(1-\frac{r^2}{G-\varphi\,\Re}\right) \quad \text{(b)} \tag{28}$$

where $\varphi=\dfrac{\mu}{4(\lambda+\mu)(\lambda+2\mu)}$,

$$G=[2n_3\mu+\lambda(n_1+n_2+n_3)]\frac{[(m_1+m_2+m_3)\lambda+2m_3\mu]}{(\lambda+2\mu)}$$

and $\Re=\min\{S,T\}$ with:

$$S=\frac{\left\{[(4m_2-2m_3)n_2-2m_2n_3]\mu+[(m_2-m_3)n_1+(m_1-2m_3+4m_2)n_2-(m_1+2m_2)n_3]\lambda\right\}^2}{(m_2-m_3)(n_2-n_3)}$$

and,

$$T=\frac{\left\{[(4m_1-2m_3)n_1-2m_1n_3]\mu+[(m_1-m_3)n_2+(m_2-2m_3+4m_1)n_1-(2m_1+m_2)n_3]\lambda\right\}^2}{(m_1-m_3)(n_1-n_3)}$$

The localization condition (25) leads, in general, to two different solutions for $\mathbf{N}_{\mathbf{crit}}$, and, therefore, to two different values for the critical angle θ_1^{crit} in Figure 7, namely:

For $S<T$:

$$\mathrm{tg}^2\theta_1^{crit}=-\frac{[(4m_3-2m_2)n_3-2m_3n_2]\mu+[(m_3-m_2)n_1+(m_1-2m_2+4m_3)n_3-(2m_3+m_1)n_2]\lambda}{[(4m_2-2m_3)n_2-2m_2n_3]\mu+[(m_2-m_3)n_1+(m_1-2m_3+4m_2)n_2-(m_1+2m_2)n_3]\lambda}$$

For $S>T$ then:

$$\mathrm{tg}^2\theta_2^{crit}=-\frac{[(4m_3-2m_1)n_3-2m_3n_1]\mu+[(m_3-m_1)n_2+(m_2-2m_1+4m_3)n_3-(2m_3+m_2)n_1]\lambda}{[(2m_3-4m_1)n_1+2m_1n_3]\mu+[(m_3-m_1)n_2+(-m_2+2m_3-4m_1)n_1+(m_2+2m_1)n_3]\lambda}$$

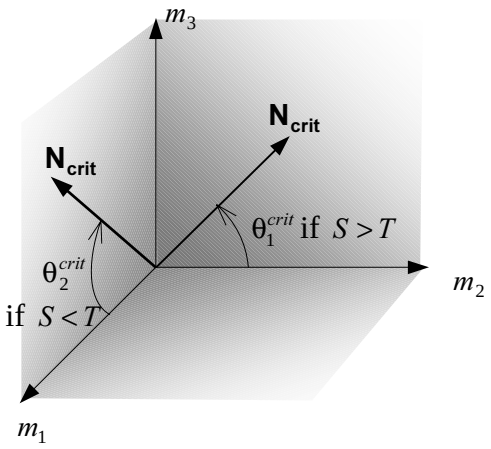

Figure 7 – Normal $\mathbf{N}_{crit}$ in the space of the principal directions of the flow tensor $\mathbf{m}$.

6 WEAK DISCONTINUITY AND BANDWIDTH LAW

The weak discontinuity regime begins as soon as the bifurcation condition $\det[\mathbf{Q}(\mathbf{N})] = \mathbf{0}$ is satisfied (bifurcation point B). Beyond this point a variable bandwidth model governs the transition between the Weak Discontinuity and the Strong Discontinuity regimes Oliver *et al.*(1998). It is given by:

$$h(q) = \begin{cases} k + \dfrac{h_B - k}{q_B - q_{SD}}(q - q_{SD}) & \text{iff} \quad q_{SD} < q \le q_B \\ k & \text{iff} \quad q \le q_{SD} \end{cases} \tag{29}$$

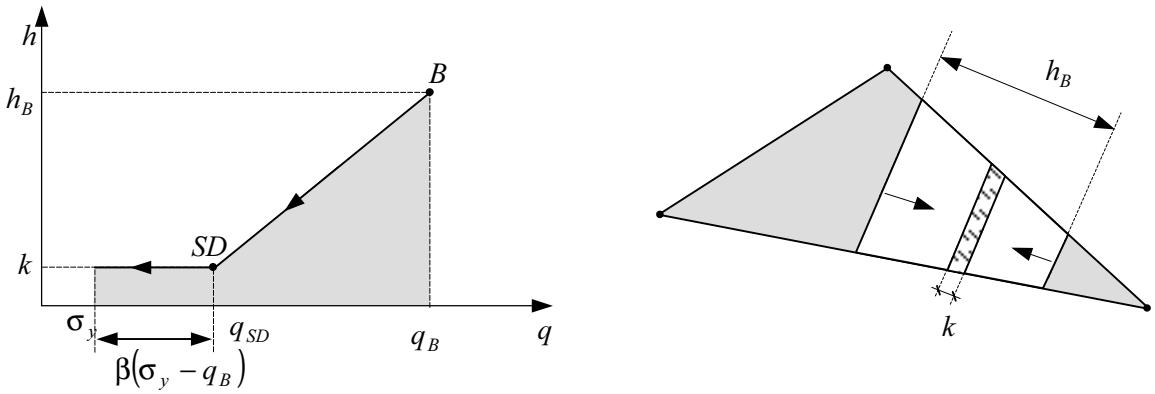

Figure 8 – Bandwidth law

Then, the continuum softening parameter $\mathcal{H}^d$ is expressed in terms of the bandwidth and the so-called discrete softening parameter $\overline{\mathcal{H}}^d$ (a material property related to the fracture energy) as:

$$\mathcal{H}^d = h\,\overline{\mathcal{H}}^d \tag{30}$$

This regularization of the softening parameter is responsible for the well posedness of the mathematical problem in the SDA, Oliver *et al.*(1998).

According to Eq. (30) the value h_B in Eq. (29) (the bifurcation bandwidth) is computed as $h_B = \mathcal{H}^d_{crit} / \overline{\mathcal{H}}^d$. The value k stands for the bandwidth at the strong discontinuity regime

that, although theoretically should be zero, is made a very small value for computational purposes (as small as permitted by the machine precision).

The strong discontinuity regime begins when the bandwidth is made zero. It can be shown that at this point the stress field at the discontinuous interface must satisfy the so-called *strong discontinuity conditions* that are specific of every constitutive model. More details can be found in Oliver (2000). Figure 9 illustrates the bandwidth evolution and the hardening/softening law.

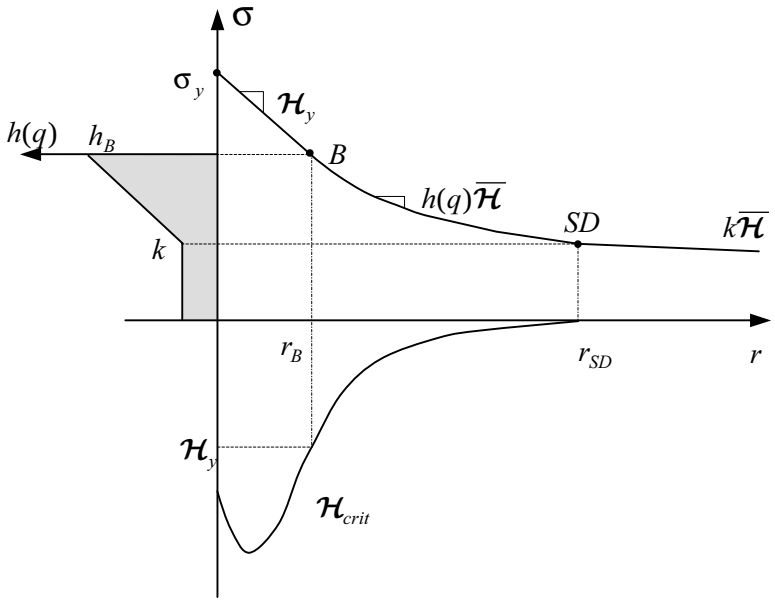

Figure 9 – Hardening/softening law and bandwidth evolution.

7 FINITE ELEMENT FORMULATION – COMPUTATIONAL ASPECTS

Motivated by the kinematics of Eq. (9) the following discrete displacement field is proposed:

$$\mathbf{u}(\mathbf{x},t) = \mathbf{N}(\mathbf{x})\,\mathbf{a}_e + M_S(\mathbf{x})\boldsymbol{\alpha}_e \tag{31}$$

where $\mathbf{N}$ contains the shape functions corresponding to the regular underlying element and $(M = H - \varphi_e)$ is the unit jump function shown in Figure 10 for two-dimensional (2D) case. In Eq. (31) φ_e is given by the combination of the shape function of the nodes which lie in the $\mathcal{B}^+$ domain, i.e.: $\varphi_e = \sum N_i \;\big|\; \forall\, i \in \mathcal{B}^+$, see Figure 11.

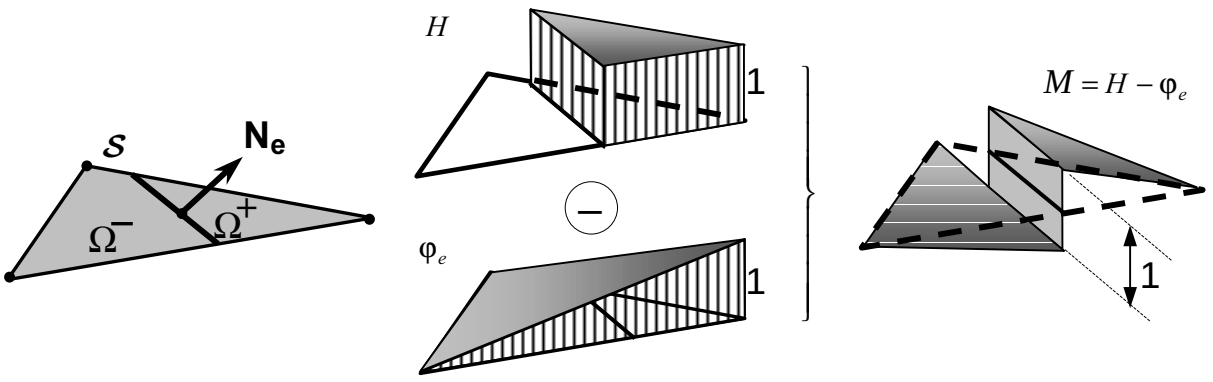

Figure 10 – Discontinuous shape function (2D case).

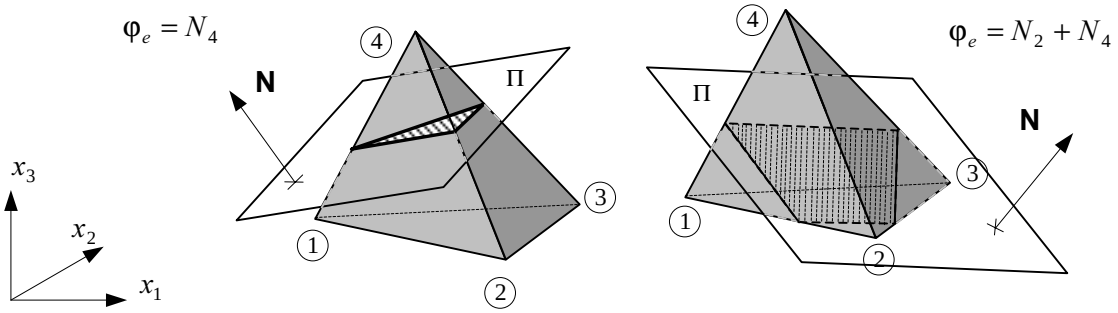

Figure 11 – Discontinuity surface and tetrahedron intersection.

From the displacement field in Eq. (31) the corresponding (rate of) strain field reads:

$$\boldsymbol{\varepsilon}(\mathbf{x},t) = \hat{\boldsymbol{\varepsilon}}(\mathbf{x},t) + \tilde{\boldsymbol{\varepsilon}}(\mathbf{x},t) = \underbrace{\mathbf{B}(\mathbf{x},t)}_{Galerkin}\mathbf{a}_e + \underbrace{\mathbf{G}_e}_{Enhanced}\boldsymbol{\alpha}_e \tag{32}$$

where the first term corresponds to the strains provided by the regular underlying element with nodal degrees of freedom $\mathbf{a}_e$ and deformation matrix $\mathbf{B}$. The second term corresponds to a strain enhancement in terms of the elemental displacement jump $\boldsymbol{\alpha}_e$ and the deformation matrix $\mathbf{G}_e$ that contains unbounded (regularized) Dirac's delta functions $\delta_{\mathcal{S}}$ emerging from the spatial derivation of the step function H in Eq. (31) namely:

$$\mathbf{G}_e(\mathbf{x}) = \begin{bmatrix} \delta_{\mathcal{S}} n_{x1} - \dfrac{\partial \varphi_e}{\partial x_1} & 0 & 0 \\ 0 & \delta_{\mathcal{S}} n_{x2} - \dfrac{\partial \varphi_e}{\partial x_2} & 0 \\ 0 & 0 & \delta_{\mathcal{S}} n_{x3} - \dfrac{\partial \varphi_e}{\partial x_3} \\ \delta_{\mathcal{S}} n_{x2} - \dfrac{\partial \varphi_e}{\partial x_2} & \delta_{\mathcal{S}} n_{x1} - \dfrac{\partial \varphi_e}{\partial x_1} & 0 \\ \delta_{\mathcal{S}} n_{x3} - \dfrac{\partial \varphi_e}{\partial x_3} & 0 & \delta_{\mathcal{S}} n_{x1} - \dfrac{\partial \varphi_e}{\partial x_1} \\ 0 & \delta_{\mathcal{S}} n_{x3} - \dfrac{\partial \varphi_e}{\partial x_3} & \delta_{\mathcal{S}} n_{x2} - \dfrac{\partial \varphi_e}{\partial x_2} \end{bmatrix} \tag{33}$$

Now the standard residual forces equation, see Zienkiewics (1996a y 1996b):

$$\mathbf{R}(\mathbf{a},\boldsymbol{\alpha}) = \mathop{\mathbf{A}}_{e=1}^{n_{el}} \left(\int_{\mathcal{B}/\mathcal{S}} \mathbf{B}^T \cdot \boldsymbol{\sigma}\, d\Omega_e - \mathbf{f}_e \right) = \mathbf{0} \tag{34}$$

where $\mathbf{A}$ is the standard finite-element assembly operator and n_{el} element number and $\mathbf{f}_e$ stands for the external forces. Equation (34) is complemented by the explicit imposition, on an element by element basis, of the inner traction continuity equation (7). This is achieved through the additional set of equations:

$$\mathbf{S}(\mathbf{a},\boldsymbol{\alpha}^{(e)}) = \int_{\Omega_e} \mathbf{G}_e^* \cdot \boldsymbol{\sigma}\, d\Omega_e = \mathbf{0} \quad \forall e = 1,...n_e \tag{35}$$

$$\mathbf{G}_e^* = \left(\delta_S - \frac{\Omega}{V_e} \right) \mathcal{N} \qquad \mathcal{N} = \begin{bmatrix} n_{x1} & 0 & 0 \\ 0 & n_{x2} & 0 \\ 0 & 0 & n_{x3} \\ n_{x2} & n_{x1} & 0 \\ n_{x3} & 0 & n_{x1} \\ 0 & n_{x3} & n_{x2} \end{bmatrix} \tag{36}$$

Finally, the elemental tangent stiffness matrix corresponding to equations (34) and (36) reads:

$$\mathbf{K}_e = \begin{bmatrix} \int_{\Omega_e} [\mathbf{B}^T \mathbb{C}^d \mathbf{B}] d\Omega & \int_{\Omega_e} [\mathbf{B}^T \mathbb{C}^d \mathbf{G}_e] d\Omega \\ \int_{\Omega_e} [\mathbf{G}^{*T}_e \mathbb{C}^d \mathbf{B}] d\Omega & \int_{\Omega_e} [\mathbf{G}^{*T}_e \mathbb{C}^d \mathbf{G}_e] d\Omega \end{bmatrix} \tag{37}$$

Matrix $\mathbf{K}_e$ is clearly non-symmetric due to the fact that $\mathbf{G}_e \neq \mathbf{G}^*_e$ in Eqs. (33) and (36). Additional details can be found in Oliver (1996a).

8 NUMERICAL RESULTS

Some numerical simulations are now presented to illustrate the application of the proposed methodology to three-dimensional problems.

8.1 Tension bar

In this example the bar of Figure 12, in a uniaxial tension process, is analyzed to investigate the mesh dependence of the results. The geometry, the boundary conditions and the material properties of the tension bar are given in the figure. The two meshes of tetrahedral finite elements shown in Figure 13 were considered: a mesh of 267 elements (mesh 1) and a much finer mesh of 1137 elements (mesh 2).
In Figure 14 the load-displacement curves obtained for both meshes are presented. It can be checked that the results are the same (indistinguishable in the plots) this showing the mesh size objectivity of the results.

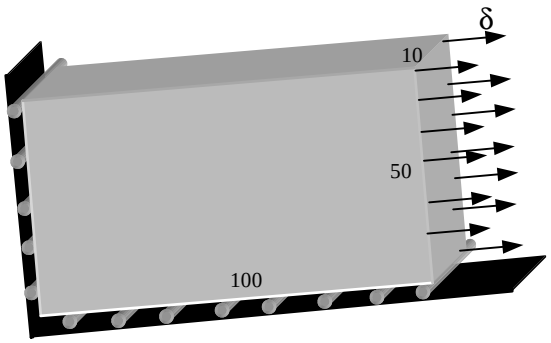

$E = 20000$
$\nu = 0.0$
$\sigma_y = 1.0$
$\mathcal{G}_f = 0.18$

Figure 12 – Tension bar.

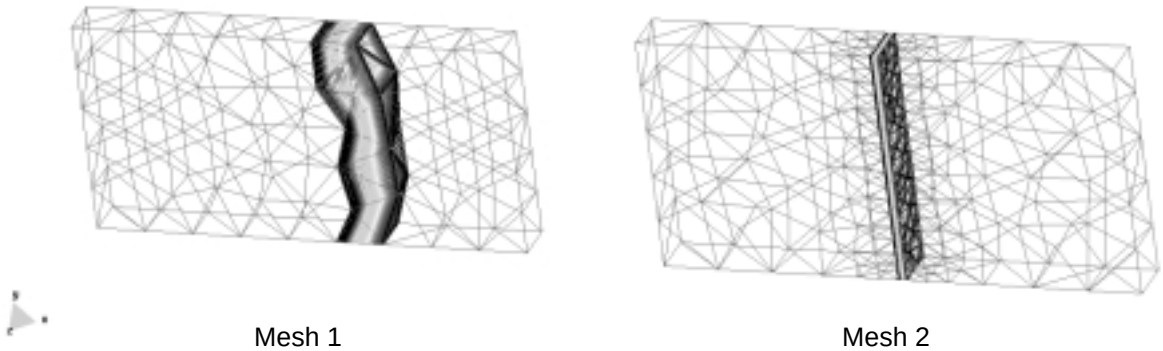

Figure 13 – Meshes and localization bands (displacement contours) for the tension bar problem.

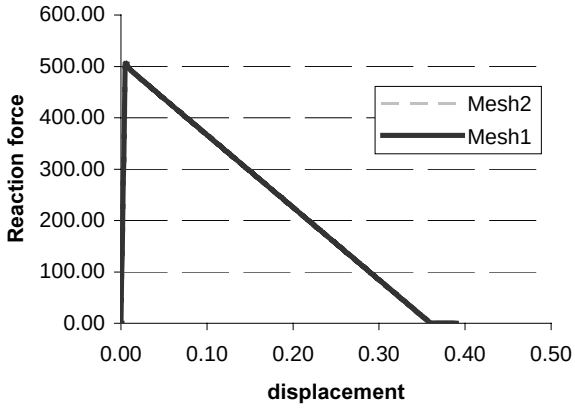

Figure 14 – Load-displacement diagram for tension bar problem.

8.2 Three-point bending test

The classical three-point bending test reported by Petersson (1981) is now tackled. The size of the specimens and the testing method are described in Figure 15 as well as the characterization of the concrete by the following parameters: fracture energy - $\mathcal{G}_f$, tensile strength - σ_y, Young's modulus - E and Poisson's ratio - ν.

Two different meshes were used to obtain the load-displacement response. Mesh 1 with 1373 elements, can be seen in Figure 16, where its deformation is shown and mesh 2 in Figure 17, with 6116 elements. Figure 18 shows the load-displacement curves for both meshes.

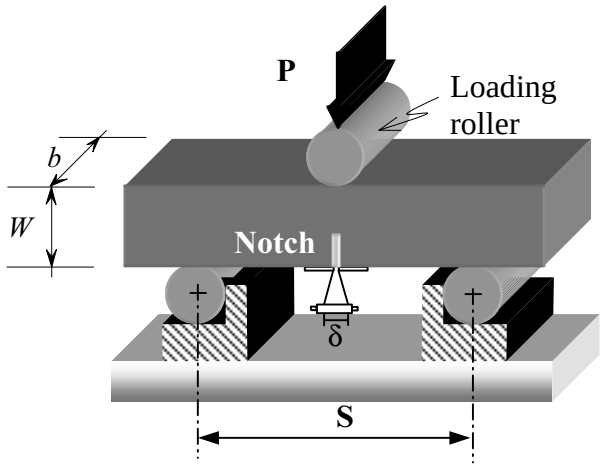

$E = 30000 N / mm^2$

$\nu = 0.20$

$\sigma_y = 3.33 N / mm^2$

$\mathcal{G}_f = 124 N / m$

$S = 2000 mm$

$b = 50 mm$

$W = 200 mm$

Figure 15 – Three point notched beam.

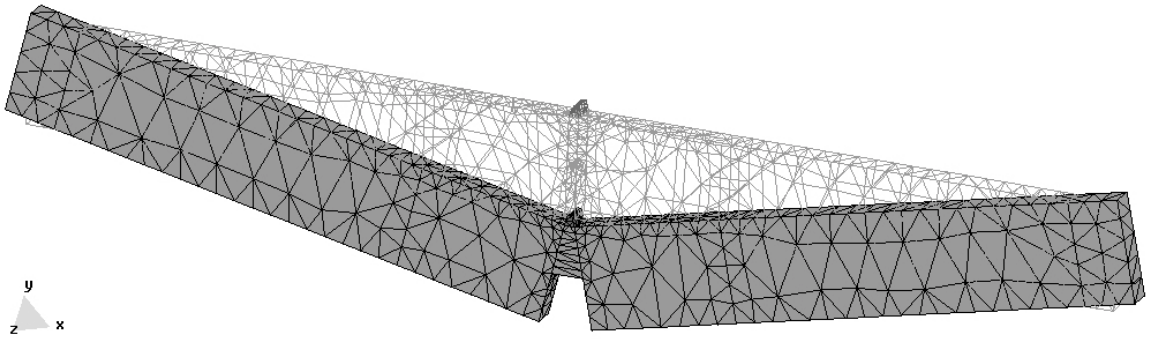

Figure 16 – Deflection – mesh 1.

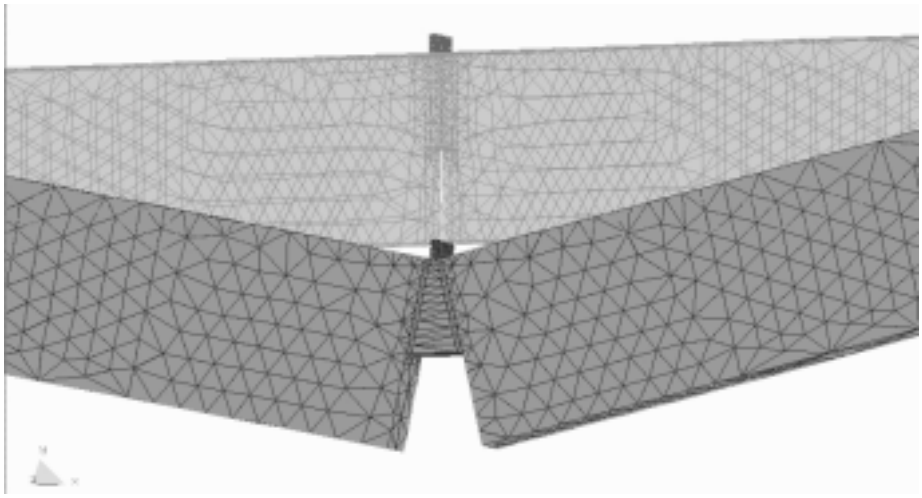

Figure 17 – Deflection – mesh 2.

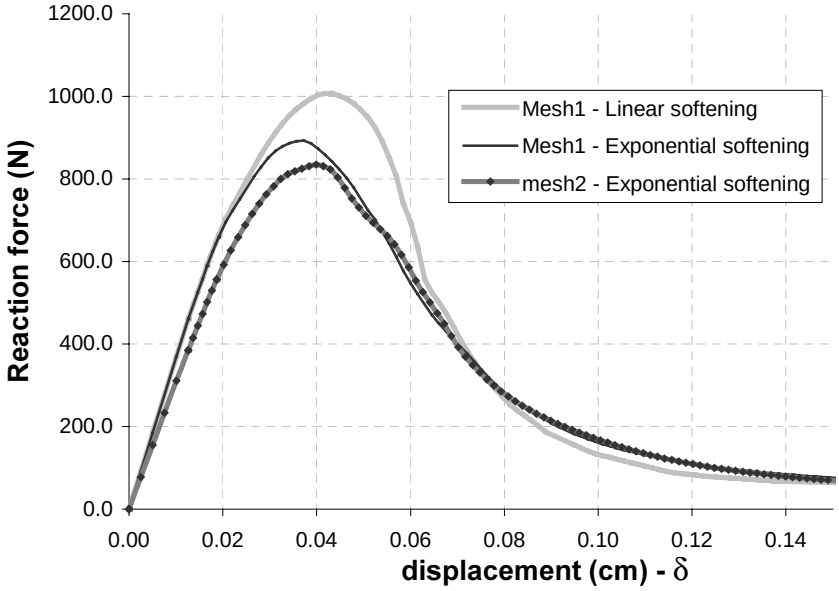

Figure 18 – Load-displacement diagram for three point notched beam.

In Figure 16 and Figure 17 the 3D original and deformed shapes of the structure are presented, for different meshes, showing the failure mode of the beam.

9 CONCLUDING REMARKS

In this paper the 3D version of the Strong Discontinuity Approach for capturing strong discontinuities has been presented. Throughout the work it has been shown that the methodology for 2D problems in Oliver(2000) can be extended to the three-dimensional case in a straight-forward manner.

The results from the bifurcation analysis, providing the discontinuity propagation directions and the critical softening parameter values, have been presented in an explicit manner suitable for computational purposes.

A tetrahedron based finite element with embedded discontinuity has been also presented. The resulting formulation has been tested in several examples showing both mesh size objectivity and ability to capture 3D failure modes.

Acknowledgment

The first author acknowledges CAPES (Brazil) its financial support and the help of Esteban Samaniego, cand. Ph.D., for his assistance and some discussions, and Dipl. –Ing. Erika Schaumann for her valuable suggestions.

REFERENCES

Armero, F. and Garikipati, K. (1996). An analysis of strong discontinuities in multiplicative finite strain plasticity and their relation with the numerical simulation of strain localization in solids. *Int. J. Solids Struct.* 33 (20-22), 2863-2885.

Bigoni, D. (2000). *Bifurcation and Instability of Non-Associative Elastoplastic Solids*. CISM Lecture Notes "Material Instabilities in Elastic and Plastic Solids", H. Petryk (IPPT, Warsaw) Coordinator, 2000.

Carpinteri, A.; Valente, S.; Zhou, F.P.; Ferrara, G. and Melchiorri, G. (1995). Crack propagation in concrete specimens subjected to sustained loads. In F.H. Wittmann (ed.) *Proceedings of the Second International Conference on Fracture Mechanics of Concrete Structures*, (FRA.M.CO.S. II): 1315-1328

Hadarmard, J. (1903). *Lenços sur la propagation des ondes et les équations de l´hydrodynamique.* Librarie scientifique, A. Hermann, Paris, France .

Hillerborg, A. (1985). Numerical methods to simulate softening and fracture of concrete. *Fracture Mechanics of Concrete. Structural Apllication and Numerical Calculation,* G. C. Sih and A. Di Tommaso, Eds., Martinus Nijhoff, Dordrecht, pp.141-169.

Ingrafea, A. R. and Saouma, V. (1985). Numerical modeling of discrete crack propagation in reinforced and plain concrete. *Fracture Mechanics of Concrete. Structural Apllication and Numerical Calculation,* G. C. Sih and A. Di Tommaso, Eds., Martinus Nijhoff, Dordrecht, pp.171-225.

Jirásek, M. (1998). Embendded crack models for concrete fracture. In de Borst *et al.*, editor, *Proc. EURO-C*. Balkema

Kachanov, L. M. (1958). Time rupture process under creep condition. Inzvestia Akademii Nauk. Otd Tech Nauk. 8, 26-31.

Kachanov, L. M. (1986). *Introduction to Continuum, Damage Mechanics*. Nijhoff, Dordrecht, The Netherlands.

Lemaitre, J. and Chaboche, J.-L. (1990). *Mechanics of Solids materials.* Cambridge University Press, Cambridge.

Manzoli, O.; Oliver, J. and Cervera, M. (1999). *Localización de deformación: Análisis y simulación numérica de discontinuidades en la mecánica de sólidos.* Centro Int. De Métodos Num. En Ingeniería (CIMNE), Monografía N. 44, Barcelona – Spain.

Münz, T.; Willam, K. and Runesson, K. (1998). Viscoplastic algorithmic operators and their localization properties. In. de Borst, Bićanić, Mang & Meschke (ed.) *Computational Modelling of Concrete Structures*. Balkema, Rotterdam.

Oliver, J. (1989). A consistent characteristic length for smeared cracking models. *Int. J. Num. Meth. Eng.*, 28:461-474, 1989.

Oliver, J. (1996a). Modelling strong discontinuities in solids mechanics via strain softening constitutive equations. Part 1: Fundamentals. *Int. J. Num. Meth. Eng.* , 39(21):3575-3600.

Oliver, J. (1996b). Modelling strong discontinuities in solids mechanics via strain softening constitutive equations. Part 2: Numerical simulation. *Int. J. Num. Meth. Eng.* , 39(21):3601-3623.

Oliver, J. (2000). On the discrete constitutive models induced by strong discontinuity kinematics and continuum constitutive equations. *International Journal Solids and Structures*, 37:7207-7229.

Oliver, J.; Cervera, M. and Manzoli, O. (1998). On the use of strain-softening models for the simulation of strong discontinuities in solids. In R. de Borst and E. van der Giessen, editors, *Material Instabilities in Solids.* John Wiley and Sons Ltd.

Oliver, J.; Cervera, M.; Oller, S. and Lubliner, J. (1990). Isotropic damage models and smeared crack analysis of concrete. In N. Bicanic et al. (ed) Proc.. *SCI-C Computer Aided Analysis and Design of Concrete Structures*, pages 945-957.

Oliver, J.; Cervera, M.; Pulido, M.D.G. and Chaves, E. (1999). "Sobre la aproximación continua de discontinuidades en mecánica de sólidos" Congreso Español de Método Numérico en Ingeniería. R. Abascal, J. Dominguez y G. Bugeda (Eds.) SEMNI, España.

Oliver, J.; Huespe, A.E.; Pulido, M.D.G. and Chaves, E. (2000). "Modelação de fissuras em estruturas de concreto mediante uma aproximação de descontinuidades fortes" *VI Congresso Nacional de Mecânica Aplicada e Computacional*, Aveiro - Portugal.

Oliver, J.; Huespe, A.E.; Pulido, M.D.G. and Chaves, E.W.V.; (2001) "From continuum Mechanics to fracture mechanics: the strong discontinuity approach". *Engineering Fracture Mechanics*. (Invited Paper).

Petersson, P. E. (1981). Crack growth and development of fracture zones in plain concrete and similar materials. Report Nº TVBM-1006, Division of Building Materials, University of Lund, Sweden.

Rice, J.R.(1976). The localization of plastic deformation. *Proc. 14th Int. Congress on Theorical an Applied Mech.*, Delft, The Netherlands, W.T. Koiter, ed., 1, 207-220.

Rots, J.; Nauta, P.; Kusters, G.M.A. and Blaauwendraad (1985). Smeared crack approach and fracture localization in concrete. *HERON*, 30(1): 48.

Rudnicki, J.W. and Rice, J.R. (1975). Condition for the localization of the deformation in pressure-sensitive dilatant material. *J. Mech. Physics of Solids,* 23, 371-394.

Simo, J. and Hughes, T.J.R. (1998). *Computational Inelasticity.* Spriner-Verlag, New York.

Simo, J. and Oliver, J. (1994a). A new approach to the analysis and simulation of strong discontinuities. In. Z.P. Bažant *et al.*, editors, *Fracture and Damage in Quasi-brittle Structures*, E&FN Spon , pages 25-39.

Simo, J. and Oliver, J. (1994b). Modelling strong discontinuities by means of strain softening constitutive equations. In H. Mang *et al.*, editor, *Proc. EURO-C 1994 Computer Modeling of concrete structures*, pages 363-372, Swansea. Pineridge Press.

Simo, J. and Rifai, S. (1990). A class of mixed assumed strain methods and the method of incompatible modes. *Int. Journ. Num. Meth. Engr.*, 29:1595-1638.

Simo, J.; Oliver, J. and Armero, F. (1993). An analysis of strong discontinuities induced by strain-softening in rate-indepedent inelastic solids. *Computational Mechanics*, 12:277-296.

Thomas, T. (1961). *Plastic flow and fracture in solids*. Academic Press, New York, N.Y.

Wells, G.N. and Sluys, L.J. (2000). Application of embedded discontinuities for softening solids. *Engineering Fracture Mechanics.* 65, 263-281.

Willam, K. (2000). *Constitutive models for materials: Encyclopedia of Physical Science & Technology*, 3rd edition. Academic Press.

Zienkiewics, O.C. and Taylor, R.L. (1994a). *El método de los elementos finitos. Volumen 1: Formulación básica y problemas lineales*. CIMNE, Barcelona, 4ª edition.

Zienkiewics, O.C. and Taylor, R.L. (1994b). *El método de los elementos finitos. Volumen 2: Mecánica de sólidos y fluidos. Dinámica y no linealidad*. CIMNE, Barcelona, 4ª edition.